<h1 style="text-align: center">Supplementary Material</h1>

1 The mono-domain Mitchell and Schaeffer model

In this section we describe how we incorporated the Mitchell and Schaeffer ionic model (MS), [1] into the 1D fiber model of atrial tissue electrophysiology. We first introduce a bi-domain description [2] of the electrophysiology by characterizing the source term with the MS model, then we re-write the equations in terms of a dimensionless potential, we introduce the mono-domain simplification and we reconstruct the extra-cellular potential from a known trans-membrane potential.

The bi-domain model introduced in [2] is written as follows:

$$\nabla \cdot (\Sigma_{\mathrm{i}} \nabla \Phi_{\mathrm{i}}) = A_{\mathrm{m}} \left(C_{\mathrm{m}} \frac{\partial V_{\mathrm{m}}}{\partial t} + I_{\mathrm{ion}} \right) \tag{1}$$

$$\nabla \cdot (\Sigma_{\mathrm{e}} \nabla \Phi_{\mathrm{e}}) = -A_{\mathrm{m}} \left(C_{\mathrm{m}} \frac{\partial V_{\mathrm{m}}}{\partial t} + I_{\mathrm{ion}} \right) \tag{2}$$

where V_{m}, Φ_{i} and Φ_{e} are the trans-membrane, intra-cellular and extra-cellular potentials respectively and are measured in mV, t is the time variable expressed in ms, $\Sigma_{\mathrm{i,e}}$ are the intra and extra cellular tissue conductivities and are expressed in S/cm, A_{m} is the cell surface per unit volume measured in cm^{-1}, C_{m} is the membrane capacitance expressed in μF/cm^2, I_{ion} is the ionic current measured in mA/cm^2. The right- and left-hand sides have units of mA/cm^3 (volumetric source).

The MS model requires scaling the potentials so that the dimensionless voltage variable v_{m} is between 0 and 1. Hence:

$$v_{\mathrm{m}} = \frac{(V_{\mathrm{m}} - V_{\mathrm{rest}})}{V_{\mathrm{ap}}}, \quad \phi_{\mathrm{i}} = \frac{(\Phi_{\mathrm{i}} - V_{\mathrm{rest}})}{V_{\mathrm{ap}}}, \quad \phi_{\mathrm{e}} = \frac{(\Phi_{\mathrm{e}} - V_{\mathrm{rest}})}{V_{\mathrm{ap}}} \tag{3}$$

where V_{ap} is the magnitude of the action potential and V_{rest} is the resting value of the trans-membrane potential, in units mV. Substituting (3) into (1), (2) and dividing by V_{ap} gives:

$$\nabla \cdot (\Sigma_{\mathrm{i}} \nabla \phi_{\mathrm{i}}) = A_{\mathrm{m}} \left(C_{\mathrm{m}} \frac{\partial v_{\mathrm{m}}}{\partial t} + \frac{I_{\mathrm{ion}}}{V_{\mathrm{ap}}} \right)$$

$$\nabla \cdot (\Sigma_{\mathrm{e}} \nabla \phi_{\mathrm{e}}) = -A_{\mathrm{m}} \left(C_{\mathrm{m}} \frac{\partial v_{\mathrm{m}}}{\partial t} + \frac{I_{\mathrm{ion}}}{V_{\mathrm{ap}}} \right)$$
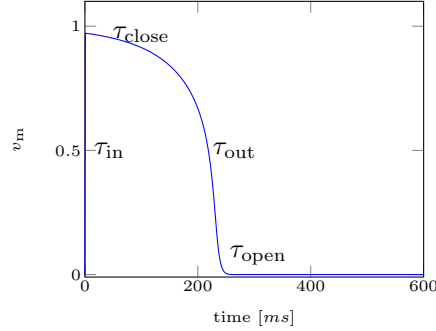
Figure 1: Parameter influence on action potential phases

and dividing by $A_{\mathrm{m}}C_{\mathrm{m}}$ gives:

$$\nabla \cdot (\sigma_{\mathrm{i}} \nabla \phi_{\mathrm{i}}) = \left(\frac{\partial v_{\mathrm{m}}}{\partial t} + J_{\mathrm{ion}} \right) \tag{4}$$

$$\nabla \cdot (\sigma_{\mathrm{e}} \nabla \phi_{\mathrm{e}}) = - \left(\frac{\partial v_{\mathrm{m}}}{\partial t} + J_{\mathrm{ion}} \right) \tag{5}$$

where $\sigma_{\mathrm{i,e}} = \Sigma_{\mathrm{i,e}}/(A_{\mathrm{m}}C_{\mathrm{m}})$ is a diffusion constant and has units of cm^2/s and $J_{\mathrm{ion}} = I_{\mathrm{ion}}/(C_{\mathrm{m}}V_{\mathrm{ap}})$ is the scaled ionic current and has units of ms^{-1}. The right- and left-hand sides of eq (4) and (5) have units of ms^{-1}. Characterizing J_{ion} by MS, subtracting equation (5) by equation (4) yields equation (6), while summing equation (5) to equation (4) yields equation (7):

$$\frac{\partial v_{\mathrm{m}}}{\partial t} = \nabla \cdot (\sigma_{\mathrm{i}} \nabla (v_{\mathrm{m}} + \phi_{\mathrm{e}})) + \frac{w v_{\mathrm{m}}^2 (1 - v_{\mathrm{m}})}{\tau_{\mathrm{in}}} - \frac{v_{\mathrm{m}}}{\tau_{\mathrm{out}}} + J_{\mathrm{stim}} \tag{6}$$

$$\nabla \cdot (\sigma_{\mathrm{i}} \nabla (v_{\mathrm{m}} + \phi_{\mathrm{e}})) + \nabla \cdot (\sigma_{\mathrm{e}} \nabla \phi_{\mathrm{e}}) = 0 \tag{7}$$

$$\frac{\partial w}{\partial t} = \begin{cases} \frac{1-w}{\tau_{\mathrm{open}}} & v_{\mathrm{m}} \le v_{\mathrm{cr}} \\ \frac{-w}{\tau_{\mathrm{close}}} & v_{\mathrm{m}} > v_{\mathrm{cr}} \end{cases} \tag{8}$$

where J_{stim} represents an externally applied current and is expressed in ms^{-1}, v_{cr} represents a threshold activation potential, taken equal to 0.13 as from the original model, τ_{in}, τ_{out}, τ_{open} and τ_{close} are the 4 characteristic times of the 4 phases of the trans-membrane potential and are expressed in ms.

The mono-domain simplification [3] considers intra- and extra- cellular conductivities proportional up to a constant λ, such that:

$$\sigma_{\mathrm{e}} = \lambda \sigma_{\mathrm{i}} \tag{9}$$

2

Introducing relation (9) into (7) and substituting into (6), it follows:

$$\frac{\partial v_{\mathrm{m}}}{\partial t} = \nabla \cdot (\sigma_{\mathrm{m}} \nabla v_{\mathrm{m}}) + \frac{w v_{\mathrm{m}}^2 (1 - v_{\mathrm{m}})}{\tau_{\mathrm{in}}} - \frac{v_{\mathrm{m}}}{\tau_{\mathrm{out}}} + J_{\mathrm{stim}} \tag{10}$$

$$\nabla \cdot (\sigma_{\mathrm{i}} \nabla \phi_{\mathrm{e}}) = -\frac{1}{1 + \lambda} \nabla \cdot (\sigma_{\mathrm{i}} \nabla v_{\mathrm{m}}) \tag{11}$$

$$\sigma_{\mathrm{m}} = \frac{\sigma_{\mathrm{i}} \sigma_{\mathrm{e}}}{\sigma_{\mathrm{i}} + \sigma_{\mathrm{e}}} = \frac{\lambda}{1 + \lambda} \sigma_{\mathrm{i}}$$

$$\frac{\partial w}{\partial t} = \begin{cases} \frac{1 - w}{\tau_{\mathrm{open}}} & v_{\mathrm{m}} \leq v_{\mathrm{cr}} \\ \frac{-w}{\tau_{\mathrm{close}}} & v_{\mathrm{m}} > v_{\mathrm{cr}} \end{cases} \tag{12}$$

where σ_{m} represents the mono-domain equivalent diffusion coefficient. We note that equations (10) and (11) are now decoupled and it is possible to solve them independently.

In this work the tissue was modeled as a thin isotropic conductor. The effect of tissue micro-structure was not considered. Due to assumed local symmetry, negligible thickness [4] and the assumption that wave curvature has a secondary effect on conduction between recording bipoles (this latter hypothesis will be verified in section 3) the model was reduced to a 1D fiber model. From (11) and the assumption of no flux of intra and extracellular currents at the boundaries, the extra-cellular potential equilibrium equation is re-written as:

$$\sigma_{\mathrm{i}} \frac{d^2 v_{\mathrm{m}}}{dx^2} + (\sigma_{\mathrm{i}} + \sigma_{\mathrm{e}}) \frac{d^2 \phi_{\mathrm{e}}}{dx^2} = 0 \qquad\qquad \sigma_{\mathrm{e}} = \lambda \sigma_{\mathrm{i}}$$

$$\sigma_{\mathrm{i}} \frac{d^2}{dx^2} (v_{\mathrm{m}} + (1 + \lambda) \phi_{\mathrm{e}}) = 0$$

$$\frac{d}{dx} (v_{\mathrm{m}} + (1 + \lambda) \phi_{\mathrm{e}}) = 0$$

$$(v_{\mathrm{m}} + (1 + \lambda) \phi_{\mathrm{e}}) = \mathrm{a} \tag{13}$$

The constant a on the right-hand side of (13) is fixed by imposing a zero spatial mean on the extra-cellular potential:

$$\overline{v}_{\mathrm{m}} = \mathrm{a}$$

$$\phi_{\mathrm{e}} = -\frac{1}{1 + \lambda} (v_{\mathrm{m}} - \overline{v}_{\mathrm{m}})$$

2 Discretization of the MS mono domain equations

To numerically solve the mono-domain Mitchell and Schaeffer equations (10) (12), we need to introduce a space discretization together with a time discretization. As far as space discretization is concerned, the trans-membrane potential v_{m} and the gate variable w were discretized with a first order Finite Element

pacing	case 1			case 2			case 3			case 4			case 5		
	CV		err (%)	CV		err (%)	CV		err (%)	CV		err (%)	CV		err (%)
	$dt=0.1$	$dt=0.01$	err (%)	$dt=0.1$	$dt=0.01$	err (%)	$dt=0.1$	$dt=0.01$	err (%)	$dt=0.1$	$dt=0.01$	err (%)	$dt=0.1$	$dt=0.01$	err (%)
0	89.7	88.6	1.3	79.5	79.1	0.5	66.7	66.0	1.0	78.7	78.2	0.6	106.1	103.7	2.3
600	83.3	82.8	0.6	76.9	76.1	1.1	60.9	60.6	0.4	76.1	76.5	−0.5	104.5	102.9	1.5
1200	84.3	82.8	1.8	76.9	76.5	0.5	61.4	60.9	0.9	76.1	76.5	−0.5	104.5	102.9	1.5

Table 1: Evaluated conduction velocity for the 5 case sets for $dt = 0.1$ (left column) and $dt = 0.01$ (center column) and relative error between the two different time resolutions (right column) Each row correspond to a each of the 3 pacing applied with an inter-pacing interval of $600\,\mathrm{ms}$.

Method (FEM) on a domain of length L $= 20\,\mathrm{cm}$ by choosing a discretization step of $dx = 200\,\mu\mathrm{m}$. The source term characterizing the ionic currents was treated with an ionic current interpolation [5]; no mass lumping was applied.

Time discretization was performed with a modification of the first order semi-implicit backward Euler method presented in [6]. A fixed time step $dt = 0.1\,\mathrm{ms}$ was chosen.

Denoting by v_{m}^n, w^n the transmembrane potential and the gating variable at time $t^n = n\delta t$, the solution at time $t^{n+1} = t^n + dt$ is obtained as follows:

1. For each node, a $0D$ Mitchell and Schaeffer ionic model with initial conditions $(v_{\mathrm{m}}^n,\ w^n)$ is discretized by a Backward Euler method and solved implicitly via Newton iterations, leading to v_{m}^*, w^{n+1}.

2. For each node, the source term of (10) is evaluated as:

$$J_{\mathrm{ion}} = \frac{w v_{\mathrm{m}}^{*^2}\left(1 - v_{\mathrm{m}}^*\right)}{\tau_{\mathrm{in}}} - \frac{v_{\mathrm{m}}^*}{\tau_{\mathrm{out}}} \tag{14}$$

3. The parabolic equation is solved with the ionic current determined in (14).

The choice of solving the parabolic diffusion equation with an implicit numerical scheme means we can avoid the restriction that the time step has to be of order $dt \simeq \left(dx^2\right)$; moreover, the solution of the ionic model by an implicit scheme avoids the time step restrictions related to the stiff character of the depolarization wave. The interested reader can find more details on [7, 8].

To ensure that we achieved a balance between numerical accuracy and speed given the large number of simulations performed we evaluated the error in the simulated conduction velocity (CV) introduced by out simulation time step. CV was calculated for each of the 5 parameter sets fitted to clinical data with the time step used in the data base $dt = 0.1$ and again with $dt = 0.01$. CV values and error are reported in Table 1. The maximum error in CV was 2.6%. This corresponds to a difference in activation times of $0.15\,\mathrm{ms}$. In context the electro grams can only be recorded at $4\,\mathrm{kHz}$ giving a $0.25\,\mathrm{ms}$ sampling interval.

s_1	case 1	case 2	case 3	case 4	case 5
300	8.2%	6.4%	6.6%	9.1%	7.0%
500	7.8%	6.7%	7.0%	7.8%	9.5%
600 (700)	7.8%	7.4%	6.9%	7.2%	8.8%

Table 2: Maximum relative error (%) on CV due to the 1D approximation compared to a 2D simulation

3 Estimation of the approximation error related to 1D modeling

The approximation of the the atrial tissue with a 1D strip neglects the curvature of the propagation front and thus introduces a modeling error. To quantify the magnitude of the error arising from this approximation, we first perform 2D numerical simulations on a $5\,\text{cm} \times 5\,\text{cm}$ slab of tissue. The same decapolar catheter described in this work was adopted and the external stimulus is applied in the center of the tissue slab, thus producing a circular propagating wave. Extracellular potentials are obtained, similarly to the 1D model as described above. From the simulated bipolar electrograms CV restitution curves were calculated. For each of the 5 parameter sets fitted to clinical data using the 1D model the CV restitution was calculated in the 2D model. The maximum absolute percentage CV error between the 1D and the 2D model for all s_2 values for a given s_1 value was used to quantify error introduced in the 1D model by ignoring potential curvature effects. The error ranges from $6.4 - 9.5\%$ with results summarized in Table 2.

4 A criterion for excluding pacemaker behavior

The MS model demonstrates pacemaker behavior, where a cell is activated in the absence of an external stimuli or diffusive currents, for specific combinations of parameter sets in 0D, 1D and 2D simulations. In 1D simulations, we test if the model is activated more times than it is stimulated to identify parameter sets that generate these ectopic beats. This is a rapid and low cost computation and is applied to all parameter sets in the data base. Any parameters sets exhibiting pacemaker behavior are removed from the data base. Testing for pacemaker behavior in 2D simulations is more computationally expensive and is only performed on parameter sets of interest. To test for pacemaker behavior a spiral wave is initiated as described in the methods section and solved for $2500\,\text{ms}$ on a coarser mesh (mean edge length of $235\,\mu\text{m}$), with the transmembrane potential and gating variable sampled every $2\,\text{ms}$. For each solution the time derivative and Laplacian of the trans-membrane potential are evaluated as follows:
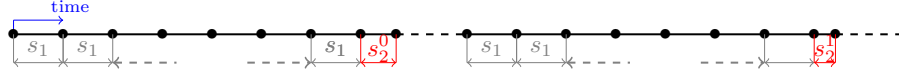
Figure 2: Example of s_1-s_2 pacing protocol. In this sequence, s_1 is kept fixed while s_2 is decremented of 20 ms

$$\frac{\partial v_{\mathrm{m}}^{n+1}}{\partial t} = \frac{v_{\mathrm{m}}^{n+1} - v^n}{dt}$$

$$\nabla^2 v_{\mathrm{m}}^{n+1} = \frac{1}{\sigma_{\mathrm{m}}} \left(\frac{\partial v_{\mathrm{m}}^{n+1}}{\partial t} - J_{\mathrm{in}}(v_{\mathrm{m}}^{n+1}, w^{n+1}) - J_{\mathrm{out}}(v_{\mathrm{m}}^{n+1}, w^{n+1}) \right)$$

For each time step we then evaluate the following conditions for all the mesh vertices:

- The voltage is increasing, $\partial v_{\mathrm{m}}^{n+1}/\partial t > 0$

- The depolarization is being driven by ionic and not diffusive currents, $\nabla^2 v_{\mathrm{m}}^{n+1} < -M$

- The cell is below the threshold value where ionic currents should not depolarize the cell, $v_{\mathrm{m}}^{n+1} < v_{\mathrm{cr}}$

where M was chosen as 2% of the maximum amplitude of the Laplacian within the whole simulation; this criterion was adopted to account for possible numerical errors in the calculation of the Laplacian.

If these three criteria are satisfied for at least one point, we consider the model to be unstable.

5 Pacing protocol definition

In this section we describe the s_1-s_2 pacing protocol adopted for evaluating tissue restitution properties. The protocol is characterized by the pre-pacing value, s_1, the initial value of the premature stimulus, s_2^0, and the decrement step for the premature stimulus, in this work taken equal to 20 ms. Once the s_1 value is chosen, the tissue is pre-paced with 8 stimuli with a temporal interval of s_1, followed by a pre-mature stimulus, s_2. The sequence, depicted in Fig. 2 for two different values of s_2, is repeated by decrementing the s_2 value down to the first value not producing an action potential. The same procedure is then repeated by considering another couple of values s_1, s_2^0; the values employed in this work are summarized in Table 3 for each case test.

6 Experimental data restitutions

In tables 4-8 CV and ERP restitutions for the 5 cases are reported. Note that, for each case and for each s_1, values reported are truncated to the first s_2

s_1 [ms]	300	500	600	700
s_2^0 [ms]	280	400	500	500
case test	1,…,5	1,…,5	1,…,4	5

Table 3: Values of s_1 and s_2^0 for characterizing the adopted pacing protocol for each of the case test

$s_1 = 600$	
500	93.33
480	92.33
460	87.5
440	87.5
420	82.35
400	70
380	65.98
360	63.62
340	61.25
320	54.45
300	44.56
280	21.88
260	0

$s_1 = 500$	
400	85.5
380	77.78
360	66.67
340	61.87
320	59.33
300	54.29
280	44.33
260	30
240	0

$s_1 = 300$	
280	54.85
260	49.99
240	46.67
220	26.56
200	0

ERP	
300	200
500	240
600	260

Table 4: Case 1 restitutions

yielding an ERP.

7 Spiral wave dynamics

In this section the predicted rotor tip path for the 5 cases is plotted in Fig. 3. The 5 cases demonstrate distinct spiral wave dynamics. Case 2 and 3 show a stable spiral wave, case 1 and 4 show a meandering spiral that break up after $t \simeq 2400\,\mathrm{ms}$ and $t \simeq 3910\,\mathrm{ms}$, respectively. Case 5 shows an unstable spiral wave that breaks up rapidly into multiple wavelets before terminating at $t \simeq 1200\,\mathrm{ms}$.

References

[1] C. Mitchell and D. Schaeffer, "A two-current model for the dynamics of cardiac membrane," *Bull. Math. Bio.*, vol. 65, pp. 767–793, 2003.

[2] L. Tung, "A bi-domain model for describing ischemic myocardial D–C potentials," Ph.D. dissertation, MIT, 1978.

[3] M. Potse *et al.*, "A comparison of monodomain and bidomain reaction-diffusion models for action potential propagation in the human heart," *IEEE Trans. Biomed. Eng.*, vol. 53, no. 12, pp. 2425–2435, 2006.

$s_1 = 600$	
500	65.33
480	65.14
460	64.9
440	64.9
420	64.14
400	63.57
380	63.14
360	62.57
340	62.14
320	59.83
300	56.91
280	52.91
260	0

$s_1 = 500$	
400	64.14
380	64.14
360	63.57
340	63.23
320	62.22
300	59.14
280	57.14
260	53.85
240	0

$s_1 = 300$	
280	62.64
260	61.22
240	57.57
220	52.85
200	0

ERP	
300	200
500	240
600	260

Table 5: Case 2 restitutions

$s_1 = 600$	
500	56.33
480	56.33
460	56.14
440	53.83
420	51.91
400	50.28
380	48.33
360	46.67
340	44.44
320	41.18
300	37.78
280	34.15
260	26.41
240	0

$s_1 = 500$	
400	55.57
380	52.83
360	50.9
340	47.46
320	45.83
300	41.42
280	38.18
260	24.54
240	0

$s_1 = 300$	
280	46.75
260	45.89
240	43.9
220	32.44
200	0

ERP	
300	200
500	240
600	240

Table 6: Case 3 restitutions

$s_1 = 600$	
500	66.64
480	66.57
460	65.33
440	64.14
420	64.33
400	63.14
380	62.9
360	61.54
340	58.64
320	57.22
300	53.12
280	0

$s_1 = 500$	
400	70.29
380	68.12
360	66.22
340	63.9
320	62.57
300	56.75
280	50.77
260	0

$s_1 = 300$	
280	67.35
260	60.49
240	52.91
220	0

ERP	
300	220
500	260
600	280

Table 7: Case 4 restitutions

$s_1 = 700$	
500	116.7
480	116.7
460	108.7
440	101
420	94.33
400	91.5
380	90.32
360	90.32
340	84.85
320	74.68
300	66.67
280	36.84
260	20.9
240	0

$s_1 = 500$	
400	92.11
380	92.11
360	87.5
340	83.33
320	79.55
300	71.43
280	63.64
260	58.33
240	0

$s_1 = 300$	
280	57.14
260	39.44
240	29.47
220	0

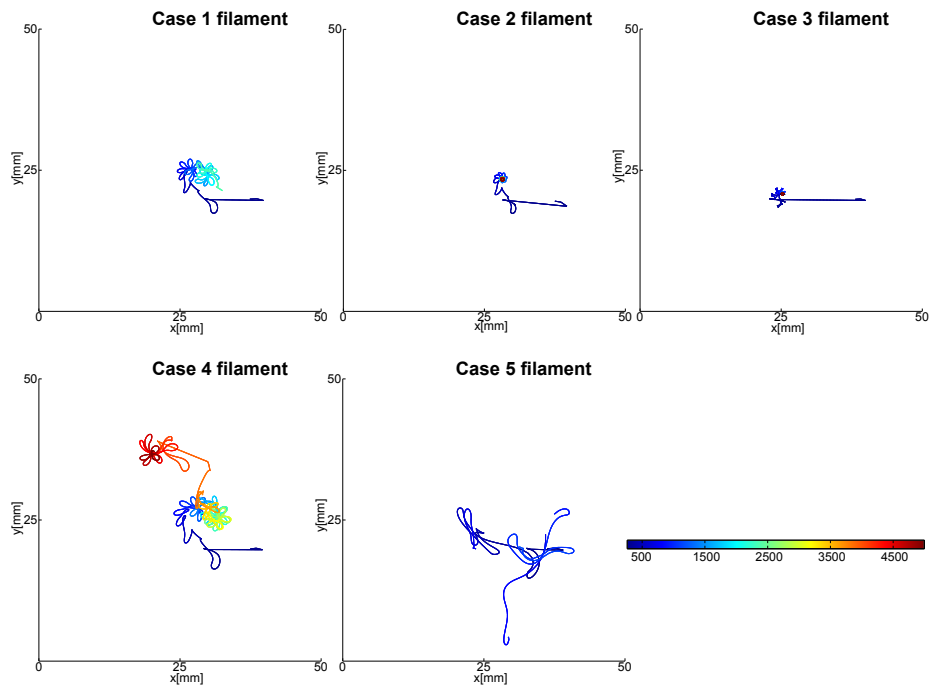| ERP	
300	220
500	240
700	240

Table 8: Case 5 restitutions

Figure 3: Path of the first filament for case 1 to 5. For cases 1, 4 and 5 filaments are plotted until break-up occurred. Case 1 and 4 rotors break up after $t \simeq 2400$ ms and $t \simeq 3910$ ms respectively. Case 5 shows an unstable spiral wave that breaks up rapidly into multiple wavelets before terminating at $t \simeq 1200$ ms. Color represents the time and is expressed in ms.

[4] M. Bishop *et al.*, "Three-dimensional atrial wall thickness maps to inform catheter ablation procedures for atrial fibrillation," *Europace*, p. euv073, 2015.

[5] P. Pathmanathan *et al.*, "Computational modelling of cardiac electrophysiology: explanation of the variability of results from different numerical solvers," *International journal for numerical methods in biomedical engineering*, vol. 28, no. 8, pp. 890–903, 2012.

[6] M. Ethier and Y. Bourgault, "Semi-implicit time-discretization schemes for the bidomain model," *SIAM J. Numer. Anal.*, vol. 46, no. 5, pp. 2443–2468, 2008.

[7] M. O. Bernabeu *et al.*, "Chaste: incorporating a novel multi-scale spatial and temporal algorithm into a large-scale open source library," *Philosophical Transactions of the Royal Society of London A: Mathematical, Physical and Engineering Sciences*, vol. 367, no. 1895, pp. 1907–1930, 2009.

[8] J. Whiteley, "An efficient numerical technique for the solution of the monodomain and bidomain equations," *IEEE Trans. Biomed. Eng.*, vol. 53, no. 11, pp. 2139–2147, 2006.